INL/CON-11-22046
PREPRINT

Parametric Evaluation of Active Neutron Interrogation for the Detection of Shielded Highly-Enriched Uranium in the Field

IEEE Nuclear Science Symposium

David L. Chichester
Scott J. Thompson
Edward H. Seabury
Ryan R. C. Clement

October 2011

The INL is a
U.S. Department of Energy
National Laboratory
operated by
Battelle Energy Alliance

Parametric Evaluation of Active Neutron Interrogation for the Detection of Shielded Highly-Enriched Uranium in the Field

David L. Chichester, *Senior Member, IEEE*, Scott J. Thompson, Edward H. Seabury, and Ryan R. C. Clement

***Abstract*– Parametric studies using numerical simulations are being performed to assess the performance capabilities and limits of active neutron interrogation for detecting shielded highly enriched uranium (HEU). Varying the shield material, HEU mass, HEU depth inside the shield, and interrogating neutron source energy, the simulations account for both neutron and photon emission signatures from the HEU with resolution in both energy and time. The results are processed to represent different irradiation timing schemes and several different classes of radiation detectors, and evaluated using a statistical approach considering signal intensity over background. This paper describes the details of the modeling campaign and some preliminary results, weighing the strengths of alternative measurement approaches for the different irradiation scenarios.**

I. Introduction

Detecting well-shielded, highly-enriched uranium (HEU) is difficult. The natural neutron emission rate of HEU, owing to spontaneous fission and (α,n) reactions is small; estimated in [1] to be 1.60 s^{-1} kg^{-1} for typical samples of HEU metal. Prior work has demonstrated the feasibility of using this signature for characterizing multiplying assemblies of shielded HEU [2]-[3]. However, the equipment needed for these measurements is large and difficult to envision using in many field-deployed applications. For passive measurements seeking to detect shielded HEU in field measurements photon-based measurements are the most used approach. The salient photon signatures for detecting shielded HEU are the 0.186-MeV gamma-ray from the decay of ^{235}U, the 0.766-MeV and 1.001-MeV gamma rays from the decay of ^{234m}Pa (a daughter product of ^{238}U, which reaches equilibrium with its parent in approximately 168 days [4]), and occasionally a 2.614-MeV gamma-ray of ^{208}Tl (a decay product of ^{232}U, which is present in uranium derived from materials formerly used in nuclear reactor fuel [5]-[6]). The 1.001-MeV photons are more penetrating then the lower-energy 0.186-MeV gamma rays but their abundance in HEU is not as high. Photons of 2.614 MeV are present in the environment naturally, since ^{208}Tl is a product in the decay chain of naturally occurring ^{232}Th, joining the chain at ^{228}Th [7]. These photons cannot, in and of themselves, be relied on as a unique indicator of HEU and they are not present at all in fresh HEU produced in modern, uncontaminated gas centrifuges.

Shielding greatly complicates the detection of HEU using passive gamma-ray measurements. Unfortunately, when considering the detection of shielded HEU, studies in this area often consider only minimal shielding, ~0.5 cm of lead, which is insufficient for fully attenuating even the low-energy gamma-rays of HEU [8]-[12]. Further, much of this prior work is predicated on the presence of ^{232}U contamination to allow passive HEU detection.

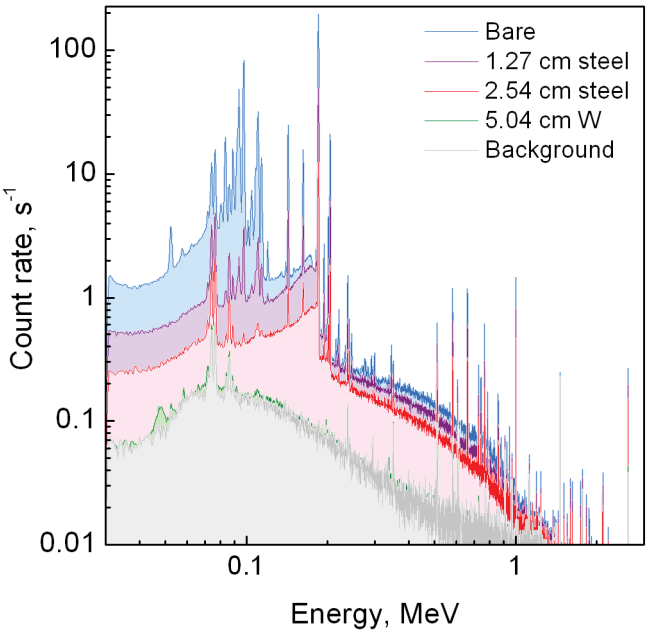

Fig. 1 Gamma-ray emission spectra, measured using a high-purity germanium spectrometer, for bare HEU and HEU shielded behind steel or tungsten. Also shown is the room background.

Although passive measurements can detect HEU under some conditions with light shielding (0.5 cm of lead (ρ = 11.34 g cm^{-3}) has an areal density of ~5.67 g cm^{-2}), they are not generally an effective technique for detecting HEU behind heavier shielding [13]. This can be understood by considering Fig. 1 which shows the passive gamma-ray spectra of a large mass of HEU bare, shielded with steel (7.8 g cm^{-3}) of thickness 1.27 cm (9.9 g cm^{-2}) or 2.54 cm (19.8 g cm^{-2}), or shielded with tungsten (19.2 g cm^{-3}) of thickness 5.04 cm

Manuscript received October 24, 2011. Idaho National Laboratory is operated for the U.S. Department of Energy by Battelle Energy Alliance under DOE contract DE-AC07-05-ID14517.

D. L. Chichester (telephone: 208-526-8920, e-mail: david.chichester@inl.gov), S. J. Thompson (telephone: 208-526-1459, e-mail: scott.thompson@inl.gov), E. H. Seabury (telephone: 208-526-5303, e-mail: edward.seabury@inl.gov), and R. R. C. Clement (telephone: 208-526-1454, e-mail: ryan.clement@inl.gov) are all with Idaho National Laboratory, Idaho Falls, Id. 83415, USA.

The author's would like to acknowledge the support of the Office of Nonproliferation and Verification Research and Development (NA-22) of the National Nuclear Security Administration, United States Department of Energy, for this work.

(96.8 g cm^{-2}). It is clear that shielding with up to 2.54 cm of steel can still permit detection of both the 0.185-MeV and 1.001-MeV gamma rays of HEU but that 5.04 cm of tungsten is truly opaque to these HEU signatures.

A close examination of the tungsten-shielded spectrum indicates a tell-tale perturbation exists, due to persistent Compton-scattered radiation and x-rays exiting the shield, but this would be very difficult to use to conclusively declare the presence of shielded HEU, or to differentiate between a shielded HEU source of radiation and other sources. Depending on other complicating factors including the background radiation environment, the presence of more complicated shields, the presence of mixed radiation sources (masking), detection time, and stand-off distance, our work has shown that shielding with an areal density of 60 to 80 g cm^{-2} is a conservative upper-boundary on the effective use of passive gamma-ray spectrometry for detecting HEU using a high-purity germanium spectrometer with measurement times on the order of an hour. In most instances considerably less shielding can effectively hide HEU from passive detection, especially for HEU-to-detector separation distances grater than a few tens of centimeters.

Active neutron interrogation (ANI) has the capability of sensing further into a shielded assembly to detect HEU [14]-[19]. ANI involves the use of a pulsed neutron source, most often an accelerator-based electronic neutron generator (ENG), to irradiate a suspect object (e.g., shipping container, pallet, storage drum, vehicle, wall, floor, etc.) with the intention of inducing fission in special nuclear material if it is present. The aim is to generate emission signatures, neutrons and photons, with sufficient intensity to be detected outside of the object. Prior work has shown that ANI can detect HEU shielded with the 'heavy' shielding defined above in short time periods of minutes to tens of minutes. However, as for passive screening, ANI also faces a limit beyond which the technique becomes ineffectual.

Recognizing that a comprehensive experimental program would be an impractical approach for trying to understand the performance capabilities and limits of ANI for detecting shielded HEU, a parametric simulation and modeling campaign is underway at Idaho National Laboratory (INL) as an alternative. This paper summarizes the parametric variables of the study, the approach used for manipulating the simulation results to represent different interrogation schemes, and the approach used for analysis. As an example, preliminary results are presented for the delayed neutron emission signature and concrete shielding.

II. Simulations

Using the MCNP family of radiation transport codes [20][21], studies were carried out to assess the neutron and photon emission signatures of fission emitted from HEU in a variety bulk shields.

A. The Model

A schematic layout of the model geometry used for the simulation is shown in Fig. 1. A 3 × 3 × 3 m^3 cube of bulk shielding material was used in each case. Seven shield matrices were studied including air, concrete, wood, polyethylene, borated polyethylene, aluminum, and steel. Highly-enriched uranium was simulated at different depths into the material from one face of the cube, from 0.2 m to 1 m. The HEU ranged in mass from 1 kg to 20 kg. Simulations were run for the HEU in the different shields alone and when surrounded by different engineered shields immediately surrounding the HEU; the engineered shields included 0.05 m of steel, 0.05 m of lead, 0.001 m of cadmium, and 0.05 m of lead surrounding the 0.001 m of cadmium. The interrogating neutron source, either monoenergetic 2.5-MeV or 14.1-MeV neutrons, was located 0.1 m outside of the cube, centered on the face closest to the HEU. A summary of the different shielding parameters is provided in Table 1.

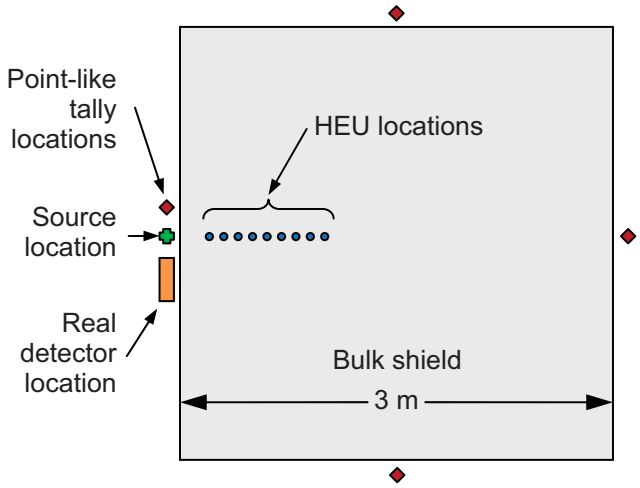

Fig. **1** Schematic layout of the model geometry, showing the relative locations of the interrogating neutron source, shielded HEU, ideal tally locations, and the real detector location.

TABLE 1. SIMULATION PARAMETERS AND VALUES

Parameter	Values
Bulk shield material	Air Concrete (2.3 g cm^{-3}) Wood (0.45 g cm^{-3}) Polyethylene (0.95 g cm^{-3}) Borated polyethylene (0.95 g cm^{-3}) Aluminum (0.6 g cm^{-3}) Steel (0.6 g cm^{-3})
Uranium mass, kg	0, 1, 2, 5, 10, and 20
Distance of uranium in the shield, m	0.2, 0.3, 0.4, 0.5, 0.6, 0.7, 0.8, 0.9, and 1
Engineered shields	None 5 cm steel 5 cm lead 0.1 cm cadmium 0.1 cm cadmium and 5 cm lead

MCNP point-like particle flux tallies were located on each side of the cube, 0.1 m from each face; on the side with the neutron source the ideal tally was 0.1 m off-center. Particle flux tallies were also determined for three idealized radiation detectors including: an array of helium-3 proportional tubes in

a polyethylene matrix, surrounded with neutron absorbing materials, to eliminate room-return thermal neutron sensitivity; a square 0.15 m × 0.15 m × 0.08 m liquid scintillator detector, and a round 5 inch × 5 inch NaI scintillator detector. For all cases results were tallied with high-resolution energy and time bins. The simulations were all run with 5×10^9 source particles. This number of particles was sufficient to ensure the simulations' precision was better than a few percent for all relevant bin tallies (time and energy) to mimic irradiations involving neutron sources with intensities 10^8 n s^{-1} with realistic background levels.

B. Modifications to Represent Interrogation

The output from the simulations corresponds to one instantaneous pulse of the interrogation source. These results must undergo several modifications to be useful for analysis. First, the time tallies are aggregated into more useful time bins, as shown in Fig. 2. Following this, the time tallies are convolved with a square pulse, to represent the duration of an actual ENG pulse, as shown in Fig. 3. Lastly, these realistic single-pulse tallies are sequentially added to one another in time to simulate the evolution of the measured signatures over the duration of a measurement. In this process, it is possible to simulate an interrogation and log the simulate/measured data as would be done in an actual measurement. Often, the signals from detectors used in active interrogation measurements are recorded using a multichannel scalar (MCS), where counts are sequentially added together in discrete time bins after a time index, usually the start of a pulse of the interrogating radiation source [18]. Using an MCS, each new pulse of the interrogation source resets the time index so that each new pulse is additive to the data of the previous pulse.

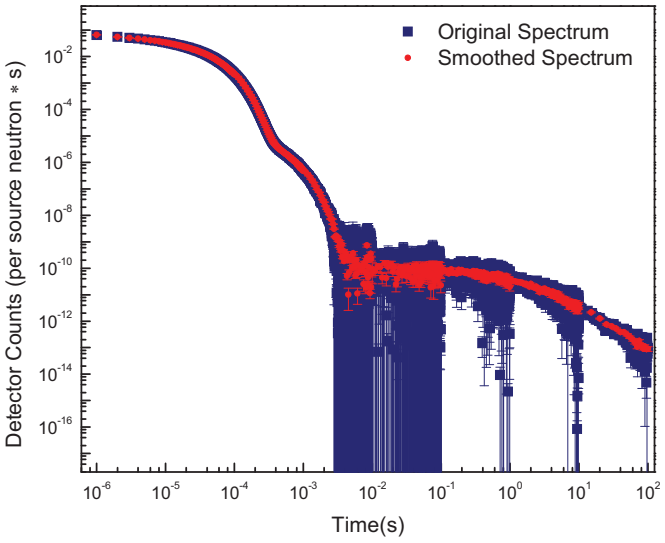

Fig. 2 An example of the raw time data and re-binned time data for a simulated neutron emission spectrum from a 5-kg mass of HEU hidden at a depth of 0.2 m within concrete, interrogated with 14.1-MeV neutrons.

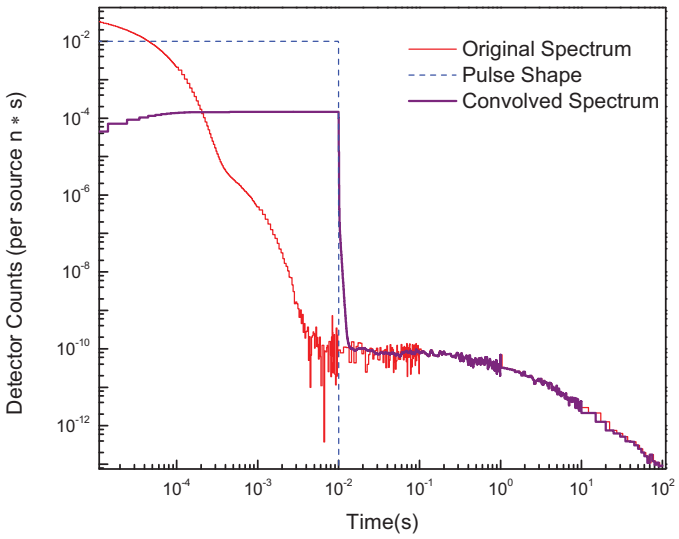

Fig. 3 The re-binned time data of Fig. 2 convolved to correspond to a single, 10-ms long ENG pulse.

In some cases all of the data is added together for the entire measurement while in other cases data might be summed together for some finite number of pulses and then reset (e.g., allowing visualization of the build-up of the delayed emission signatures). The simulation reconstruction employed here allows for the replication of the experiments when using an MCS. Rather than using an MCS, experimental data from active interrogation measurements is sometimes tabulated individually, as 'list-mode' mode data. The summations performed for this analysis do not allow for re-analysis in list mode.

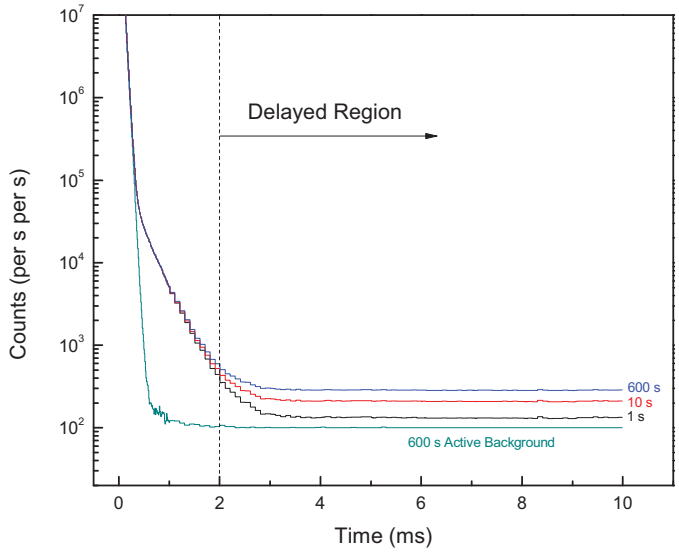

Fig. 4 Simulated MCS spectra for 1 (black), 10 (red), and 100 (blue) second measurements using a 14.1 MeV source to interrogate 5 kg of HEU 0.02 m within concrete. The no-HEU case is shown in green. A passive background rate of 1 count per second was applied.

An example of the final output of the simulation post-processing algorithms is shown in Fig. 4 for simulated

measurements made with the ^{3}He detector module. The ENG pulsed at a frequency of 1000 Hz with a duty cycle of 1% (100 μs pulse width).

For analysis different time and energy cuts may be made on the tally data, to represent the real-world performance of different types of detectors. For the simulation shown in Fig. 4, for example, a time cut has been introduced at 2 ms after the start of the ENG pulses. The net signal would then be calculated on a second-by-second basis from 2 ms to 10 ms to indicate the intensity and statistical precision of an observation to observe delayed neutrons (in this case). For active interrogation it is possible to perform a passive background measurement prior to an interrogation but it is not possible to perform an active background measurement; that is, one cannot measure the scenario in a known empty configuration. Therefore, it is important to choose detectors and observables where the background signals in the observed region (both energy and time) are invariant to local irradiation conditions. This is often easily done when measuring β-delayed neutrons using detectors shielded against thermal neutrons. For β-delayed gamma rays this often necessitates waiting longer than 10 ms (at a minimum) to allow residual thermal neutrons present in the shield, and their associated capture gamma rays, to be completely gone prior to the collection of data.

III. Analysis Approach

The modeling approach has been designed to generate a simulated count signal versus time which evolves over the course of each simulated experiment. Our approach for analyzing the results of the simulations is based upon the concept of setting a threshold signal value referred to as a decision level. Measurements above the decision level are classified as a positive detection measurement, while those signals below the threshold are considered a negative detection.

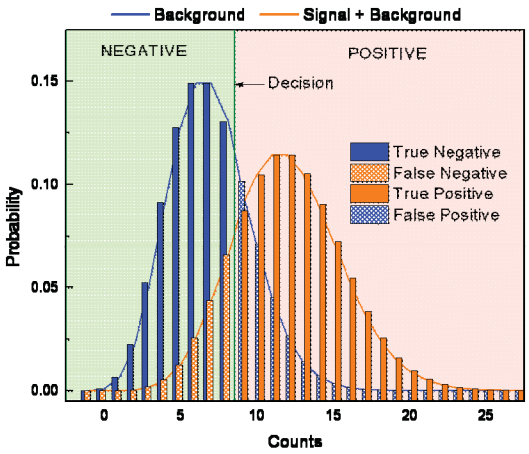

Fig. 5 Probability distribution functions for a 7 count background and a 5 count signal (12 counts total). A decision level of 9 counts is implemented in the figure to demonstrate how probabilities for each of the four detection outcomes are calculated.

This is illustrated by considering an example measurement where a background measurement of 7 counts is compared to an interrogation value of 5 counts (measured as 12 total counts including background). For these two measurements probability distributions may be determined following Poisson statistics such that the probability of measuring n counts, given a mean signal value of S (7 and 12 in this case), is given by (1). Unlike standard Gaussian (Normal) probability distributions, the Poisson distribution is not continuous, but provides discrete probabilities for whole-integer measurement totals. These two distributions are shown in Fig. 5.

$$P(n,S) = \frac{S^{n}\, e^{-S}}{n!} \tag{1}$$

A decision level of 9 counts was implemented for the example shown in Fig. 5, marked by a green line. Measured totals of 9 counts and above fall into the positive detection category, highlighted with orange in the figure. Conversely, counts of 8 and below fall into the green highlighted negative-outcome portion of figure. Once a decision level is set, a given inspection measurement can have four possible detection outcomes.

- True Negative: Clandestine material is not present. The signal is measured below the decision level and correctly identified as a negative detection.
- False Negative: Clandestine material is present. The signal is measured below the decision level and misclassified as a negative detection. This is also referred to as a "Miss."
- True Positive: Clandestine material is present. The signal is measured above the decision level and correctly identified as a positive detection.
- False Positive: Clandestine material is not present. The signal is measured above the decision level and misclassified as a positive detection. This is also referred to as a "False Alarm."

The likelihood for each of these four outcomes can be determined using the calculated probability distributions. Integrating the background and signal distributions below the decision threshold provides the negative outcome probabilities, while integrating above it will give the probabilities for the positive outcomes.

From a computational standpoint, these integrations can be determined by implementing numerical methods to solve the incomplete gamma function. However, we have found no benefit to calculation speed or accuracy for such an implementation. Thus, simple summing methods were employed for these calculations. Fig. 5 also demonstrates how the outcome probabilities are interrelated. With properly normalized distributions the sum of true negative and false positive probabilities and the sum of false negative and true positive probabilities should both be equal to unity.

A. The ROC Curve

The proper choice for the decision level is often a compromise between the operational requirements for a given detection application. An increase in decision level will reduce false alarms at the cost of sensitivity. Conversely, a

decrease in decision will reduce the number of missed detections, but increases the operational burdens of false alarm escalation. Hence, decision is often a dynamic and somewhat arbitrary quantity, adjusted to suit measurement scenario parameters. A measurement-to-measurement comparison should take into account all circumstances, providing a complete evaluation of overall "detectability." The receiver operating characteristic (ROC) analysis, commonly employed in medical research communities, is just such a method that graphically summarizes the four detection outcome probabilities for all possible decision conditions.

A ROC curve is essentially a plot of false positive versus true positive detection rates, yet the complementary nature of the four detection outcome probabilities allows for the concurrent demonstration of false negative and true negative rates as well. Examples of these types of plots are shown in Fig. 6. Absolute detectability can be defined as having a 100% probability rate for both of the true detection outcomes with no chance for the false outcomes. On a standard ROC scale this is represented by the upper-left most corner of the plot. Hence, a ROC curve's level of concavity in this quadrant is indicative of the corresponding measurement scenario's sensitivity. The ROC analysis method can also be useful in determining an application-appropriate decision level, since each point on the curve corresponds to a single decision level setting. Advancing the decision is equivalent to a movement in outcome-probability space, along the ROC curve, toward the false positive-true positive origin. This analysis can therefore be used as a guide for adjusting the decision to meet the situational requirements of a given measurement.

Receiver operating characteristic curves are being generated for each simulation in this project, for different signatures, under different irradiation and background conditions. The Poisson nature of the generated probability distributions limits decisions to nonnegative integer values. Once a decision level is reached that corresponds to a null false positive fraction, all subsequent decision values will result in the same. Hence, distributions that span a greater number of counts, that is those distributions with higher mean values, offer a larger number of possible decisions with which to sample and construct the ROC curve. This trend is demonstrated clearly in Fig. 6, it contains time evolving ROC analyses for the 14.1 MeV neutron interrogation (DT generator source) of a 10-kg mass of highly enriched uranium (HEU) hidden at a depth of 50 cm within a bulk concrete volume.

B. Decision Criteria

While insightful and informative, the receiver operating characteristic method provides a somewhat abstract analysis of measurement sensitivity. In field deployable detection applications, decision levels are often calibrated to acceptable operational costs incurred from false alarms. Hence, a pragmatic analysis approach is to hold either the false positive or the false negative probability constant, and monitor how the other false fraction behaves as a function of measurement time. This is a variation on the methods presented by Currie [22].

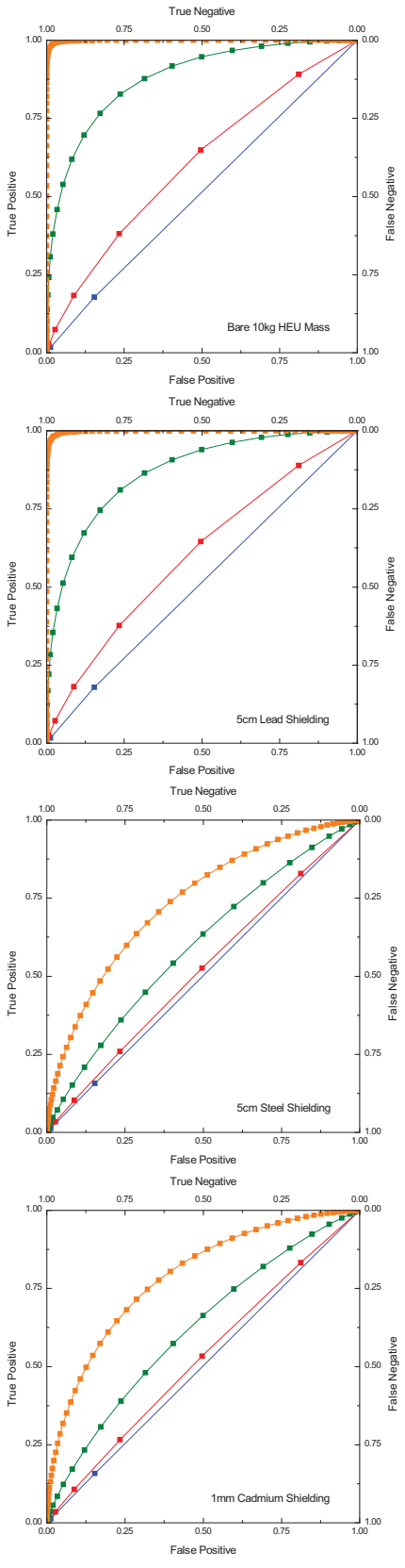

Fig. 6 ROC curves for 14.1 MeV neutron interrogation of a 10-kg mass of HEU positioned at a depth of 0.5 m in bulk concrete. Each plot of the figure corresponds to a different near-shield configuration. Curves are provided for 1 second (blue), 10 second (red), 100 second (green), and 600 second (orange) measurements, with a 10 counts per minute neutron background.

Such an analysis was performed, holding the false positive rate at 5, 2, 1, and 0.1%, and reporting false negative rates for each of the four cases in Fig. 6. With decision levels restricted to integer values, convergence routines must be employed to solve the inverse incomplete gamma function for the decision value that most closely results in the assigned false positive rate without surpassing it. Hence, the declared false positive values serve more as a maximum limit rather than a constant in this analysis. Fig. 7 contains four examples of the data sets generated by this analysis. These plots of miss rate versus measurement time are for a 5-kg mass of HEU hidden at a depth of 0.2 m in the concrete volume, with the false positive limit set at 1%. On the macroscopic scale, as measurement times increase beta-delayed signature intensities increase, statistical uncertainties are reduced, and false negative rates drop dramatically. However, these plots also contain some level of microstructure that stems from the non-continuous Poisson-nature described above. As measurement time increases, the probability-distribution mean values (averages), which are not restricted to integer values, increase as well. Hence, for a given decision value, the false positive rate slowly increases closer to the limiting value. Once that limit is reached, the decision value must be incrementally increased for false alarm rates to stay below this limit, forcing steep and regular decreases in the calculated false positive fractions. As illustrated in the figure, the results of these decision shifts are observed as periodic jumps in the reported false negative rates.

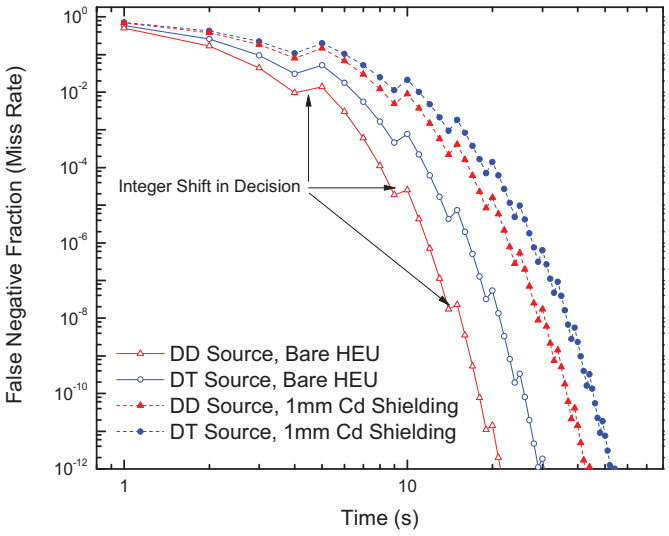

Fig. 7 Calculated false negative detection rates as a function of measurement time for the interrogation of a 5-kg mass of HEU hidden at a depth of 0.2 m within the bulk concrete shielding. Values are provided for measurements using 2.5 MeV (DD) and 14.1 MeV (DT) neutron sources, with and without 1 mm of cadmium surrounding the uranium target. False negative values are provided for decision levels that result in a maximum false positive rate of 1%.

Following the generation of the time-dependent false negative distributions, several miss rate thresholds were selected to serve as stop triggers for a time based analysis process. Each distribution was evaluated for the measurement time in which the false negative values fall below each of the thresholds. This allowed for the accumulation of groups of data sets into mass-variable, time-dependent distributions. Examples of these data sets are provided in Fig. 8 and Fig. 9.

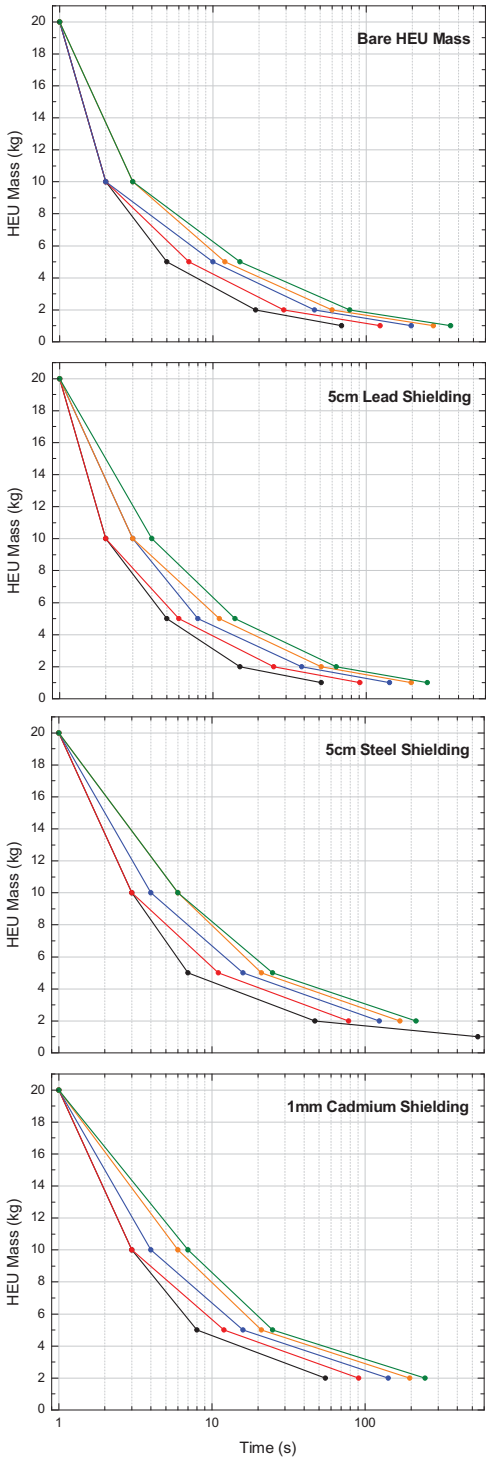

Fig. 8 Detectable mass versus measurement time for false negative confidence levels of 5% (black), 1% (red), 0.1% (blue), 0.01% (orange), and 0.001% (green) with a false-positive detection rate held below 0.1%. HEU masses were simulated at a depth of 0.2 m within the cement volume and were interrogated with 14.1 MeV neutrons with a passive background rate of 10 counts per minute. Each plot of the figure corresponds to a different near-shield configuration.

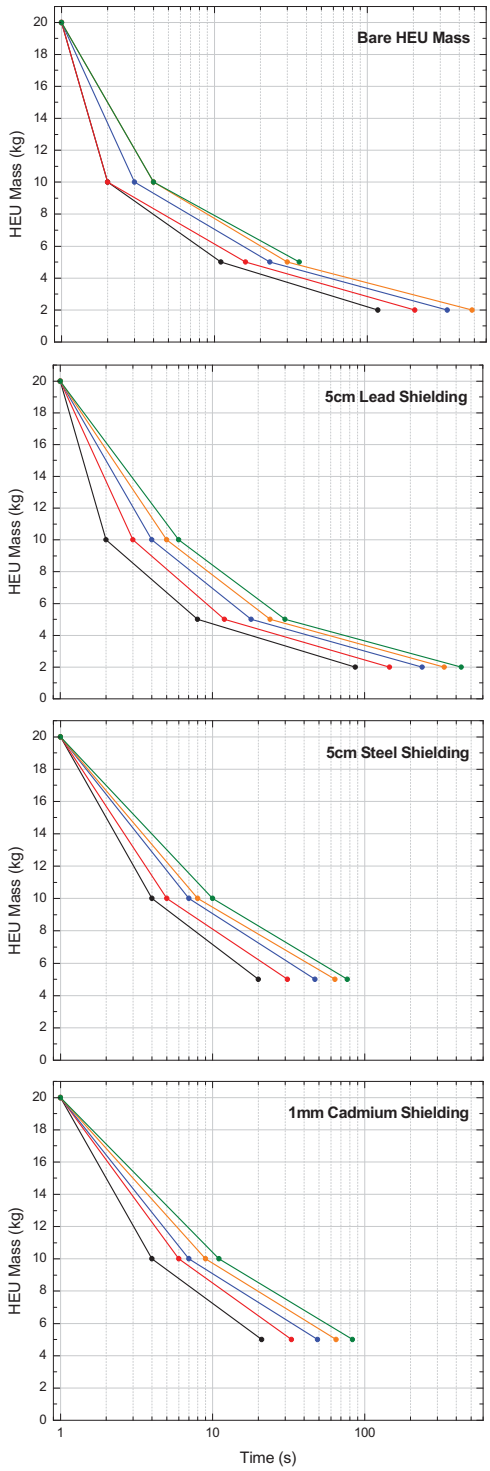

Fig. 9 The same as Fig. 8 but with a passive background rate of 100 counts per minute.

These figures contain plots of detectable mass versus measurement time for several miss rates. This presentation of the statistical data clearly illustrates measurement sensitivity in a manner that emphasizes accessibility and practicality.

Detectable mass versus measurement time plots for the 14.1 MeV neutron interrogation (yield = 10^8 n s^{-1}, frequency = 100 Hz, duty cycle = 10%) of HEU hidden at a depth of 20 cm in the concrete volume is shown in Fig. 8. These data sets assume a passive background level of 10 counts per minute, and false alarm rates were held at or below 0.1%. Each plot of this figure contains data for a single near-shield configuration. The calculations used here are for the delayed neutron signature, as measured with a polyethylene-moderated helium-3 detector, using 4 atm. tubes, a detector surface area of approximately 0.22 m^2, and an intrinsic detection efficiency of approximately 10.8% for bare, fission-spectrum neutrons.

A single kilogram of HEU can be detected in 70 s with a false negative fraction of 5% but to decrease the miss rate down to 0.001% the inspection time must be increased to at least 350 s under these measurement parameters. It is clear here again that with a 14.1 MeV source neutron energy, the implementation of a 5-cm thick lead shield around the HEU does little in the way of retarding the beta-delayed neutron signature. Indeed, the neutron multiplicative nature of lead actually aids in the detection process for smaller HEU masses. The steel and cadmium near-shields push required inspection times for 1-kg sensitivities beyond the 600 s boundary of this analysis in all but the 5% false negative case for 5 cm of steel.

The data sets presented in Fig. 9 are similar to those shown in Fig. 8 but with an increase in passive background levels from 10 to 100 counts per minute. This has a dramatic effect on the minimal detectable mass limits within the 600 s inspection time constraint of this analysis. A single kilogram is no longer detectable in these measurement scenarios with the reported confidence levels. Only with the presence of a 5-cm lead shield can 2 kg be detected with a 0.001% miss rate. The use of 5 cm of steel, or 1 mm of cadmium, reduces the minimal detectable mass to 5 kg for all the false negative condition levels.

IV. Summary

A research program is underway at Idaho National Laboratory to investigate the bounds of applicability for active neutron interrogation to detect shielded highly-enriched uranium. This analysis is focused on conditions relevant for the use of portable instrumentation for field applications, which limits the choice of interrogating radiation to the use of compact electronic neutron generators producing either 2.5-MeV or 14.1 MEV neutrons. Recognizing that high-resolution gamma-ray spectrometers are frequently used in passive screening, and that reasonably long measurement times would be available for using an HPGe detector to screen a suspected object to detect the 1.001-MeV or 0.766-MeV gamma-rays associated with the decay of the ^{234m}Pa daughter product, ANI should at a minimum be able to detect HEU behind more 100 g cm^{-2} of shield material in order to be relevant for field use. Unfortunately, research in this area frequently fails to focus on this level of shielding in assessments of ANI for field work.

Acknowledging the complexity of carrying out a comprehensive experimental campaign to study this topic, we have initiated a simulation and modeling campaign to help understand the far bounds of ANI, beyond the 100 g cm^{-2} level. This modeling considers a number of different bulk

shield-engineered shield combinations, as well as multiple interrogation signatures including prompt (die-away) and β-delayed neutrons and delayed gamma-rays. Analysis of the results of these simulations is performed using statistics familiar to those understanding the ROC curve methodology for signal analysis. As a figure of merit for comparing different problems the time needed to detect a shielded mass of HEU is being used, with either the maximum acceptable false-positive rate or the maximum acceptable false-negative rate being used as a constraint.

A preliminary result, which is shown here, is that in a concrete shield with an HEU mass hidden 0.2 m inside, detection of 2 kg or more of HEU can be achieved within 300 seconds with a very low false positive rare, and reasonably false-negative probabilities, using one small detector (having a 10 count per minute background rate) observing the delayed-neutron signature, even with the presence of several different types of engineered shields. If the background rate is ten times larger, however, the minimum detectable mass under the same conditions is generally degraded to 5 kg. It should be highlighted that, for these examples, a very low false-positive (FP) rate was chosen as the constraint. This low FP rate, perhaps suitable for high through-put screening, may not be suitable for situations where only one or two measurements may be needed. In such cases the minimum detectable mass in the same measurement periods would be much lower.

Preliminary tests have shown the correctness of the simulation approach used for this work. An example of these results is shown in Fig. 10. As a part of this project further benchmarking experiments are planned at INL to help validate the modeling used in these studies. These experiments will be performed at INL using large 1 m × 1 m × 1 m cubes specifically designed for this purpose with HEU masses varying from 1 kg to 10 kg. Polyethylene-moderated helium-3 neutron detectors, liquid scintillators, and sodium iodide scintillators will be used as detectors.

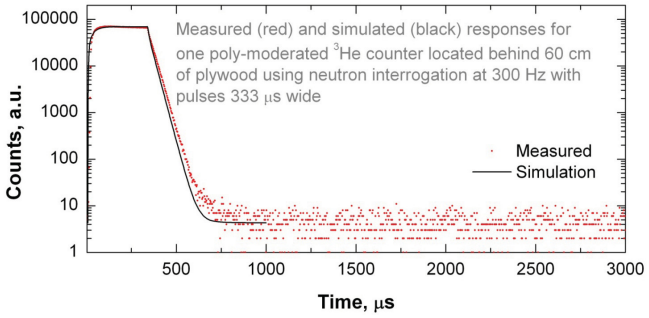

Fig. 10 Comparison of the simulated and measured die-away response of a polyethylene-moderated helium-3 detector system to irradiation with a deuterium-tritium ENG.

REFERENCES

[1] Fetter, S., et al., "Detective Nuclear Warheads," Sci. Global Sec. 1 (1990) 225-302.

[2] Verbeke, J. M., et al., "Testing of Liquid Scintillator Materials for Gamma and Neutron Detection," Report LLNL-CONF-414602, Lawrence Livermore National Laboratory, Livermore, Calif. (2010).

[3] Nakae, L. F., et al., "Recent Development in Neutron Detection and Multiplicity Counting with Liquid Scintillator," Report LLNL-CONF-422505, Lawrence Livermore National Laboratory, Livermore, Calif. (2010).

[4] Yücel, H., Çetiner, M. A., and Demirel, H., "Use of the 1001 keV Peak of ^{234m}Pa Daughter of ^{238}U in Measurement of Uranium Concentration by HPGe Gamma-Ray Spectrometry," Nucl. Inst. Meth. Phys. Res. A 413 (1998) 74-82.

[5] Peurrung, A. J., "Predicting 232U Content in Uranium," Report PNNL-12075, Pacific Northwest National Laboratory, Richland, Wash. (1998).

[6] Lemley, J. R., et al., "Confirmatory Measurements for Uranium in Nuclear Weapons by High-Resolution Gamma-Ray Spectrometry (HRGS)," Report BNL-66293, Brookhaven National Laboratory, Upton, N. Y. (1999).

[7] Oberer, R. B., et al., "The Use of Tl-208 Gamma Rays for Safeguards, Nondestructive-Assay (NDA) Measurements," Report Y/EN-8270, Y-12 National Security Complex, Oak Ridge, Tenn. (2009).

[8] Phlips, B. F., et al., "Comparison of Shielded Uranium Passive Gamma-Ray Detection Methods," Proc. SPIE 6213 (2006) 62130H.

[9] Keyser, R. M., Upp, D. L., and Twomey, T. R., "Performance of an Improved HPGe-Based Radioisotope Identifier (RIID) in the Identification of SNM and SNM Mixtures," Proc. 47th Annual Meeting of the Inst. Nucl. Mat. Manage., Nashville, Tenn,, July (2006).

[10] Wulf, E. A., "Compton Imager for Detection of Special Nuclear Material," Nucl. Inst. Meth. Phys. Res. A 579 (2007) 371-374.

[11] "American National Standard Performance Criteria for Hand-Held Instruments for the Detection and Identification of Radionuclides," Standard ANSI N42.34-2006, IEEE, New York, N.Y. (2007).

[12] Hofstetter, K. J., Beals, D. M>, and Odell, D. M., "Uranium Detection Using Small Scintillators in a Maritime Environment," J. Radioanal. Nucl. Chem. 276 (2008) 433-439.

[13] Doyle, J. E., *Nuclear Safeguards, Security, and Nonproliferation*, Oxford, U.K., Butterworth-Heinemann (2008) 511-512.

[14] Brodzinski, R. L., Dietrich, D. D., Geelhood, B. D., Hilton, N. R., Jones, J. L., McKinney, G. W., Micklich, B. J., Mihalczo, J. T., Moss, C. E., Okada, C. E., Sanger, H. M., Slaughter, D. R., and Todosow, M., " Evaluation of Active Interrogation Techniques for Detecting Special Nuclear Material in Maritime Cargo Containers," Report PNNL-15722, Pacific Northwest National Laboratory, Richland, Wash. (2003).

[15] "Preventing and Defending Against Clandestine Nuclear Attack," Report of the Defense Science Board Task Force, Office of the Undersecretary of Defense for Acquisition, Technology, and Logistics, U.S. Department of Defense, Washington, D. C., June (2004)

[16] Moss, C. E., Hollas, C. L., McKinney, G. W., and Myers, W. L., "Comparison of Active Interrogation Techniques," IEEE Trans. Nucl. Sci. 53 (2006) 2242-2246.

[17] "Detecting Nuclear and Radiological Materials," RS Policy Document 07/08, The Royal Society, London, U.K., March (2008).

[18] Chichester, D. L. and Seabury, E. H., "Using Electronic Neutron Generators in Active Interrogation to Detect Shielded Fissionable Material," IEEE Trans. Nucl. Sci. 56 (2009) 441-447.

[19] Chichester, D. L. and Seabury, E. H., "Addressing Different Active Neutron Interrogation Signatures from Fissionable Material," IEEE Nucl. Sci. Symp. Conf. Rec., Orlando, Fla., October 25-31 (2009) 956-960.

[20] "MCNP—A General Monte Carlo N-Particle Transport Code, Version 5," Report LA-UR-03-1987, Los Alamos National Laboratory, Los Alamos, N.M. (2003).

[21] "MCNPX—A General Purpose Monte Carlo Radiation Transport Code, Version 2.5.0, MCNPX User's Manual," Report LA-UR-05-0369, Los Alamos National Laboratory, Los Alamos, N.M. (2005).

[22] Currie, L. A., "Limits for Qualitative Detection and Quantitative Determination," Anal. Chem. 40 (1968) 586-593.